IEEE Access
Multidisciplinary ⋮ Rapid Review ⋮ Open Access Journal

Received May 6, 2022, accepted June 1, 2022, date of publication June 9, 2022, date of current version June 20, 2022.

Digital Object Identifier 10.1109/ACCESS.2022.3181725

A Filter Structure Based Broadband Electrical Impedance Matching Method for Piezoelectric Transducer of Acoustic Well-Logging

YONGCHAO YAO[1], (Member, IEEE), BAOHAI TAN[2], ZHANXIANG HE[3,4], AND XIANPING LIU[5]

[1]Department of Earth and Space Sciences, Southern University of Science and Technology, Shenzhen 518055, China
[2]School of Geosciences, China University of Petroleum (East China), Qingdao 266580, China
[3]Shenzhen Key Laboratory of Deep Offshore Oil and Gas Exploration Technology, Southern University of Science and Technology, Shenzhen 518055, China
[4]Guangdong Provincial Key Laboratory of Geophysical High-Resolution Imaging Technology, Southern University of Science and Technology, Shenzhen 518055, China
[5]CNPC Logging Company Ltd., Tianjin Branch, Tianjin 300280, China

Corresponding author: Zhanxiang He (hezx@sustech.edu.cn)

This work was supported in part by the Shenzhen Science and Technology Program under Grant KQTD20170810111725321, in part by the Shenzhen Key Laboratory of Deep Offshore Oil and Gas Exploration Technology under Grant ZDSYS20190902093007855, in part by the Guangdong Provincial Key Laboratory of Geophysical High-resolution Imaging Technology under Grant 2022B1212010002, in part by the Shandong Provincial Natural Science Foundation under Grant ZR2018BD023, and in part by the Fundamental Research Funds for the Central Universities under Grant 18CX02176A.

ABSTRACT Piezoelectric transducer is a key component of acoustic well-logging tool. Transducers used in acoustic well-logging tools usually have limited bandwidth, and their dominant frequencies severely drift with drastic change of borehole temperature when tools are working downhole. An appropriate impedance matching is necessary to broaden the operating bandwidth of the transducer and improve the power output stability of the acoustic emission. In this study, an electrical impedance matching (EIM) method for piezoelectric transducer is proposed based on Butterworth response and network theory. The method can broaden the bandwidth of narrowband transducers while ensuring stable transducer power gain (TPG). A band-pass filtering circuit and its low-pass prototype are constructed on the basis of the equivalent circuit of the piezoelectric transducer and the external impedance matching circuit. According to the filtering characteristics of the filter circuit and a target TPG function, we derive the analytical formulas for calculating power transmission characteristics and electronic component values of arbitrary order matching network. Using different electronic design automation (EDA) software, we simulated the matching network of a specific transducer obtained by the theoretical calculations. Then, we built an experimental system to verify the performance of the matching network. Theoretical calculation, simulation and experimental results demonstrate that the impedance matching network obtained by the proposed method can effectively broaden the operating bandwidth of narrowband transducers and provide stable output power.

INDEX TERMS Piezoelectric transducer, Butterworth response, electrical impedance matching, two-port network, acoustic well-logging.

I. INTRODUCTION

Acoustic well-logging is a commonly used geophysical method to acquire formation lithology and physical properties. In engineering, the acoustic emission (AE) system of logging tool emits acoustic pulses to the formation. Then, the acquisition system acquires the acoustic signals propagated through the formation. Finally, the formation lithology and physical properties are obtained by inversion calculations according to the acquired acoustic signal. To improve the signal-to-noise ratio (SNR) of the received signals and ensure the accuracy of inversion calculations, the AE system should have high and stable output power.

Acoustic transducers with high mechanical quality factor (Q_m) are usually adopted in logging tools to ensure the AE efficiency. The relation $\Delta f = f_0/Q_m$ indicates that the bandwidth of this type of transducer is narrow. Due to the influence of geothermal gradient (1–3 °C /100 m), borehole temperature increases with well depth. Thus, the operating temperature range of the logging tool is large and may exceed 200 °C [1]–[3].

The associate editor coordinating the review of this manuscript and approving it for publication was Yingxiang Liu.

The performance (especially impedance characteristics) of piezoelectric transducers is significantly influenced by ambient temperature. Through heating experiments, we obtain the frequency–conductivity curves of a given narrowband transducer at different ambient temperatures (Fig. 1). The figure shows that the impedance–admittance characteristics of transducers are sensitive to temperature variation. The drastic temperature change leads to the drift of central frequency (ω_c). As a result, the inconsistency between the frequency of the excitation signal and the center frequency of a narrowband transducer causes the decrease in excitation efficiency, which also weakens the power output stability of AE systems.

The key to solve the problem is to broaden the operating band of the transducer while ensuring stable output power. For a given narrowband transducer, the primary method to achieve this goal is to match the transducer with an external impedance circuit. The two common impedance matching methods are: electronic design automation (EDA) method and analytical method [4]–[11]. EDA methods such as Smith Chart analysis, real frequency technique, and direct optimization are widely used in high frequency applications, such as RF (300 kHz − 300 GHz) circuits. However, these methods cannot guarantee that the obtained matching network is optimal. Different from that, the central frequency of piezoelectric transducer adopted in conventional acoustic well-logging is usually less than 30 kHz, which is much lower than that of the high frequency applications.

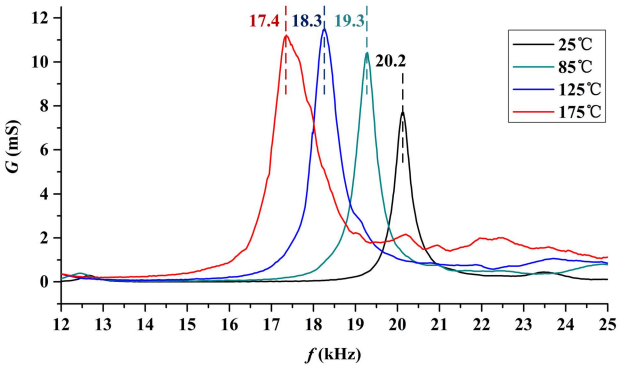

FIGURE 1. The measured impedance characteristic (admittance) curves of the given piezoelectric transducer at different temperatures.

In impedance matching, the equivalent electrical model of a common piezoelectric transducer can be regarded as a sample RLC load. Then, the mathematical analytic of the transducer's matching circuit can be derived based on the assumption of a target transducer power gain (TPG) function [12]–[14]. Thus, a general mathematical analytic method based on the flattest filter response is introduced in the following parts to realize the broadband electrical impedance matching for low-frequency piezoelectric transducers.

II. BUTTERWORTH RESPONSE CHARACTERISTICS AND TWO-PORT MATCHING NETWORK

The matching network proposed according to the design requirements should not only broaden the bandwidth of the transducer, but also improve the in-band flatness of TPG. Actually, these requirements are consistent with the filtering characteristics of some common passive filters.

According to the characteristics of common passive filters, Butterworth filter has the flattest amplitude-frequency response and most stable TPG under the same filtering order n and -3-dB (half-power) angular frequency bandwidth BW_n. Therefore, the filtering response of the ideal band-pass Butterworth filter is chosen as the target TPG function $G(s)$. In complex plane, the function $G(s)$ can be expressed as

$$G(s) = \frac{K_n}{1 + (-y^2)^n} \tag{2.1}$$

where $s = j\omega$ is complex frequency, $y = (s + \omega_c^2/s)/BW_n$ is the normalized low-pass-to-band-pass conversion, and the maximum attainable gain constant K_n represents the output power gain at the frequency $\omega = \omega_c$.

To design a matching circuit and make the power output characteristics of transducer meet with (2.1), we first analyze the impedance characteristics of the transducer. According to Butterworth–Van Dyke (BVD) model [15], [16], the equivalent circuit of a piezoelectric transducer is shown in Fig. 2, where R_1, C_1, L_1, and C_2 represent dynamic resistance (mechanical loss resistance), dynamic capacitance, dynamic inductance, and static capacitance, respectively.

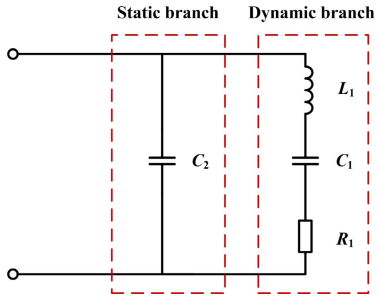

FIGURE 2. BVD equivalent circuit model of piezoelectric transducer.

The BVD model shows that the impedance of the dynamic branch is $Z_D = R_D + jX_D = R_1 + j(\omega L_1 - 1/\omega C_1)$. Taking no account of the internal resistance of signal source, to minimize Z_D, the excitation signal with frequency $\omega_s = 1/\sqrt{L_1 C_1}$ is used to excite the transducer to make $X_D = 0$ and $|Z_D| = R_D$. In this case, series-resonance occurs in the dynamic branch, thereby allowing the dynamic branch to act as a pure resistance [17], [18]. Hence,ω_s is called the series resonant angular frequency, and ω_s of a narrowband transducer usually approximates the central frequency ω_c. However, when series-resonance occurs in the dynamic branch, the impedance of the static branch is $Z_S = -j/\omega_s C_2$, thereby making the entire equivalent circuit still capacitive.

As shown in Fig. 3, the common matching method at ω_s sets an appropriate parallel inductance L_2 on the static branch and makes the impedances of C_2 and L_2 conjugate to compensate for the influence of C_2, which means that

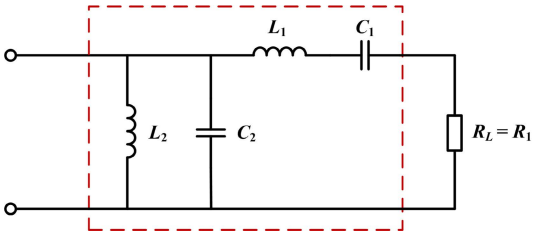

FIGURE 3. Equivalent single-frequency-point matching circuit for piezoelectric transducer.

$j\omega_s L_2 - j/\omega_s C_2 = 0$. Further derivation shows that

$$L_2 C_2 = L_1 C_1 = 1/\omega_s^2. \tag{2.2}$$

When using a certain excitation source, the single-frequency-point matching can endow the most effective power output at $\omega = \omega_s$. However, the disadvantages of this matching method emerge when applied for narrowband transducers. In particular, the output power of the transducer is low at non-resonant frequency. When ω_s drifts with changes in temperature, the effect of impedance matching and AE efficiency also worsens.

If the dynamic resistance R_1 is regarded as a pure resistive load R_L, then the active power of the transducer P_L is actually the power consumed by R_L. When we regard the network composed of C_1, L_1, C_2, L_2, and other components as an n-order passive filter, the problem of electrical impedance matching for piezoelectric transducer becomes a design problem of the n-order filter. For a specific pure resistive load R_L, the power output characteristics of the filter meet (2.1).

Let E_S and R_S be the voltage and internal resistance of a constant voltage signal source, respectively, and introducing other filtering elements of the mentioned n-order filters into Fig. 3, then we propose the broadband matching circuit, as shown in Fig. 4. Similar to (2.2), the impedances of L_k and C_k in the same circuit branch should be conjugated to endow the most effective power output at $\omega = \omega_s$, that is,

$$L_k C_k = L_1 C_1 = 1/\omega_s^2, (k \in N^*, k \geq 2) \tag{2.3}$$

In this circuit, the equivalent component values of the transducer are certain, while $R_S, L_k (k \in N^*, k \geq 2)$, and $C_k (k \in N^*, k \geq 3)$ are unknown. The problem now is to obtain R_S and the unsolved components of the arbitrary order filter according to (2.1), (2.3), and the known parameters of the given transducer (ω_s, R_1, L_1, C_1, and C_2). The equivalent broadband matching circuit is determined, then BW_n and K_n can be obtained by further derivations.

By removing the inductance of the parallel branch and the capacitance of the series branch in Fig. 4, we can obtain low-pass prototype of the equivalent broadband matching circuit (see Fig. 5).

According to Youla [19], the ladder band-pass structure composed of L_k and C_k can be regarded as a lossless two-port network N, then we can redraw Fig. 5 as Fig. 6, where $p = yBW_n = s + \omega_c^2/s$ represents the frequency conversion from a band-pass filter to its low-pass prototype. $Z_{11}(p)$ is the

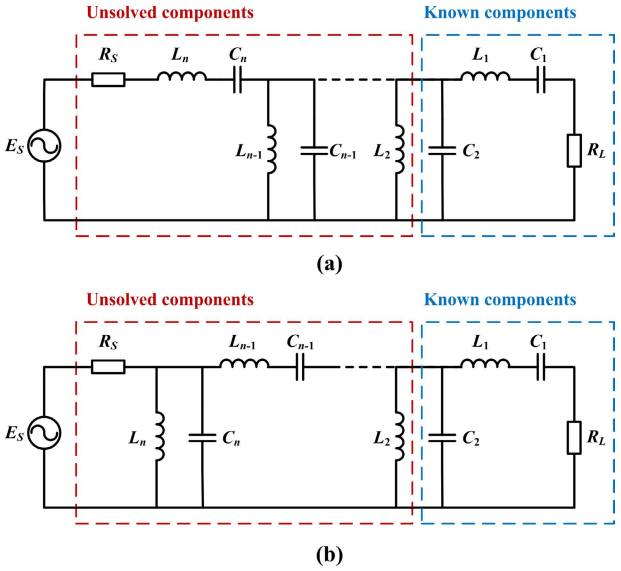

FIGURE 4. Equivalent broadband matching circuit for piezoelectric transducer. (a) n is odd, (b) n is even.

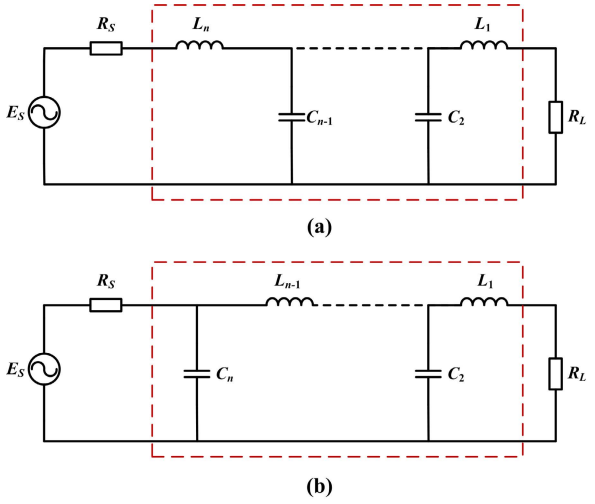

FIGURE 5. Low-pass prototype of the equivalent broadband matching circuit for piezoelectric transducer. (a) n is odd, (b) n is even.

input impedance that looks toward the input terminal "11", and it is also known as the driving-point impedance function.

Let $S_{11}(p)$ and $S_{21}(p)$ be the input reflection coefficient of port 1 and the forward transmission coefficient of port 1 to port 2, respectively. Then,

$$S_{11}(p) = [Z_{11}(p) - R_S]/[Z_{11}(p) + R_S], \tag{2.4}$$

$$|S_{11}(p)|^2 = 1 - |S_{21}(p)|^2. \tag{2.5}$$

The relation $|S_{21}(p)|^2 = G(s)$ is established because network N has the same power output characteristics as the n-order Butterworth filter. By substituting (2.1) into (2.5) and performing analytic continuation yield, we can obtain that

$$S_{11}(p)S_{11}(-p) = 1 - |S_{21}(p)|^2 = 1 - G(s) = \frac{1 - K_n + (-y^2)^n}{1 + (-y^2)^n}. \tag{2.6}$$

Let $\delta = (1 - K_n)^{1/2n}$ and $x = y/\delta$, then the minimum-phase solution of (2.6) [20] is as follows:

$$S_{11}(p) = \pm\delta^n \cdot q(x)/q(y), \tag{2.7}$$

where Hurwitz polynomial

$$q(y) = \sum_{k=0}^{n} a_k y^k. \ (0 \le k \le n) \tag{2.8}$$

Let $\alpha = \pi/2n$, then the coefficients of this polynomial have the following features and recursive relation

$$\begin{aligned} a_0 &= 1, \\ a_k &= a_{n-k}, \\ a_{k+1} &= a_k \cos k\alpha / \sin(k+1)\alpha, \\ a_{n+1} &= 0. \end{aligned} \tag{2.9}$$

The following formula can be obtained by transforming (2.4)

$$Z_{11}(p) = R_S \frac{1 + S_{11}(p)}{1 - S_{11}(p)}. \tag{2.10}$$

Then, $Z_{11}(p)$ can be obtained by substituting (2.7) into (2.10). However, the sign of $S_{11}(p)$ must be first determined.

Consider the first order of the matching network in Fig. 5 must be the inductance L_1 in series with R_L. Then, according to the series–parallel connections among the circuit components, we can conclude that

$$Z_{11}(p) = \begin{cases} L_n p + \cfrac{1}{C_{n-1}p + \cfrac{1}{L_{n-2}p + \cfrac{1}{\ddots + \cfrac{1}{L_1 p + R_L}}}}, & n \text{ is odd} \\ C_n p + \cfrac{1}{L_{n-1}p + \cfrac{1}{C_{n-2}p + \cfrac{1}{\ddots + \cfrac{1}{L_1 p + R_L}}}}, & n \text{ is even} \end{cases} \tag{2.11}$$

The reactance characteristics of inductance and capacitance indicates that the sign of reflection coefficient $S_{11}(p)$ depends on the parity of matching network order n. When n is odd, the sign is positive; otherwise, it is negative. $Z_{11}(p)$ can be expressed with Hurwitz polynomial $q(y)$ by substituting (2.7) into (2.10). To simplify expressions and facilitate subsequent discussions, (2.10) is rewritten as follows:

$$Z_{11}(p) = \begin{cases} R_S \cdot \dfrac{\sum_{k=0}^{n} a_k(1+\delta^k)y^{n-k}}{\sum_{k=1}^{n} a_k(1-\delta^k)y^{n-k}}, & n \text{ is odd} \\ R_S \cdot \dfrac{\sum_{k=1}^{n} a_k(1-\delta^k)y^{n-k}}{\sum_{k=0}^{n} a_k(1+\delta^k)y^{n-k}}, & n \text{ is even} \end{cases} \tag{2.12}$$

The Hurwitz polynomial coefficients features in (2.9) and the transformation $k = n - k'$ are utilized in the derivation of (2.12).

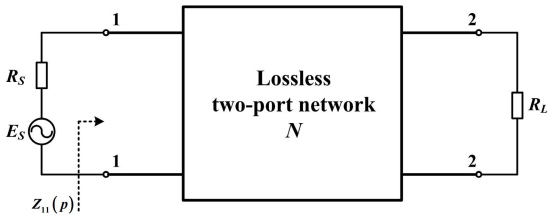

FIGURE 6. Schematic of the lossless two-port matching network.

To study the correspondence between the two expression forms of $Z_{11}(p)$ in (2.11) and (2.12), we transform (2.12) into the following continued fraction. According to recursion algorithm and Euclidean algorithm,

$$\frac{Z_{11}(p)}{R_S} = g_n y + \cfrac{1}{g_{n-1}y + \cfrac{1}{g_{n-2}y + \cfrac{1}{\ddots + \cfrac{1}{g_1 y + g_0}}}}, \tag{2.13}$$

where g_k $(k \in N^*, 0 \le k \le n)$ is the impedance constant associated with the components of respective circuit branch, and its value is related to the parity of n. Based on (2.11) and (2.13), the correspondences between g_k and L_k, or correspondences between g_k and C_k are

$$\begin{aligned} R_L &= R_1 = g_0 \cdot R_S, \\ &\begin{cases} L_1 p = g_1 y \cdot R_S, \\ C_2 p = g_2 y / R_S, \end{cases} \\ &\vdots \\ &\begin{cases} L_k p = g_k y \cdot R_S, & k > 2, k \text{is odd} \\ C_k p = g_k y / R_S, & k > 3, \ k \text{is even} \end{cases} \end{aligned} \tag{2.14}$$

(2.14) indicates that if $g_0, g_1, g_2, \ldots, g_n$ are determined by the known transducer parameters, then other unknown components in the EIM circuit can be obtained. The detailed derivations and calculations will be presented in Section III.

III. DERIVATION AND CALCULATION

The expression of g_k should be first obtained to determine the unknown components in the matching circuit. We define a polynomial function serial $A_m(y)(m \in N^*, 0 \le m \le n)$ and let the order of $A_{m+1}(y)$ be lower than that of $A_m(y)$ by one. Replacing $A_m(y)$ with A_m in the following discussions to simplify expression, then the following relations among the items in the polynomial function series are obtained:

$$\begin{aligned} A_{m-1}/A_m - A_{m+1}/A_m &= g_{n-m+1}y, \ 0 < m < n \\ A_{n-1}/A_n - A_{n+1}/A_n &= g_1 y + g_0. \end{aligned} \tag{3.1}$$

Let

$$\begin{aligned} A_0 &= \sum_{k=0}^{n} a_k(1+\delta^k)y^{n-k}, \\ A_1 &= \sum_{k=1}^{n} a_k(1-\delta^k)y^{n-k}. \end{aligned} \tag{3.2}$$

Substituting (3.2) into (2.12), then using Euclidean algorithm, mathematical induction, and (3.1), we can obtain the expressions of any polynomial function A_m and constant g_{n-m+1} as follows:

$$A_m = B_m \sum_{k=m}^{n} a_k C_{m,k} D_{m,k} y^{n-k}, \tag{3.3}$$

$$g_{n-m+1} = 2\sin(2m-1)\alpha \cdot B_{m-1}/B_m,\ 0 < m \le n \tag{3.4}$$

where

$$C_{m,k} = \begin{cases} 1, & m = 0,\ m = 1 \\ \prod_{p=1}^{m-1} \dfrac{\sin(k-p)\alpha}{\sin(k+p)\alpha}, & m > 1 \end{cases} \tag{3.5}$$

$$D_{m,k} = \begin{cases} 1+\delta^k, \\ \qquad m = 0 \\ \sum_{p=0}^{k-1} \delta^p, \\ \qquad m = 1 \\ \sum_{p=0}^{k-m} \prod_{q=1}^{m-1} \dfrac{\sin(p+q)\alpha}{\sin q\alpha} \cdot \dfrac{\sin(k-p-q)\alpha}{\sin(k-q)\alpha} \cdot \delta^p, \\ \qquad m > 1 \end{cases} \tag{3.6}$$

$$\begin{aligned} B_m &= [\delta^2 - 2\delta\cos(2m-2)\alpha + 1] \cdot B_{m-2},\ \ m \ge 2 \\ &= \begin{cases} 1, & m = 0 \\ 1-\delta, & m = 1 \\ \prod_{p=1}^{m/2} [\delta^2 - 2\delta\cos(4p-2)\alpha + 1], & m \ge 2, \\ \qquad m \text{ is even} \\ (1-\delta) \prod_{p=1}^{(m-1)/2} [\delta^2 - 2\delta\cos 4p\alpha + 1], \\ \qquad m \ge 3,\ m \text{ is odd} \end{cases} \end{aligned} \tag{3.7}$$

$$B_n = \begin{cases} 1-\delta^n, & n \text{ is odd} \\ 1+\delta^n, & n \text{ is even} \end{cases}$$

$$B_{n-1} = \begin{cases} (1+\delta^n)/(1+\delta), & n \text{ is odd} \\ (1-\delta^n)/(1+\delta). & n \text{ is even} \end{cases} \tag{3.8}$$

To simplify the discussion, the detailed proofs of (3.3) to (3.8) are presented in APPENDIX I.

(3.3) to (3.8) are the bases of subsequent derivation of network parameters and components. (3.4) indicates that constant g_{n-m+1} is associated with the division B_{m-1}/B_m. To obtain the general expression of g_k, we derive g_0, g_1, and g_2 at first.

According to (3.4) and (3.8), we can obtain

$$\begin{aligned} g_1 &= 2\sin(2n-1)\alpha \cdot B_{n-1}/B_n, \\ &= \begin{cases} 2(1+\delta^n)\sin\alpha/[(1+\delta)(1-\delta^n)], & n \text{ is odd} \\ 2(1-\delta^n)\sin\alpha/[(1+\delta)(1+\delta^n)]. & n \text{ is even} \end{cases} \end{aligned} \tag{3.9}$$

Substituting (3.9) into (3.1) yields

$$\begin{aligned} g_0 &= (1+\delta) \cdot B_{n-1}/B_n \\ &= \begin{cases} (1+\delta^n)/(1-\delta^n), & n \text{ is odd} \\ (1-\delta^n)/(1+\delta^n). & n \text{ is even} \end{cases} \end{aligned} \tag{3.10}$$

(3.4), (3.7), and (3.8) demonstrate that

$$\begin{aligned} g_2 &= 2\sin(2n-3)\alpha \cdot B_{n-2}/B_{n-1} \\ &= [2\sin 3\alpha/(\delta^2 + 2\delta\cos 2\alpha + 1)] \cdot B_n/B_{n-1} \\ &= \begin{cases} \dfrac{2(1+\delta)(1-\delta^n)\sin 3\alpha}{(1+\delta^n)(\delta^2+2\delta\cos 2\alpha+1)}, & n \text{ is odd} \\ \dfrac{2(1+\delta)(1+\delta^n)\sin 3\alpha}{(1-\delta^n)(\delta^2+2\delta\cos 2\alpha+1)}. & n \text{ is even} \end{cases} \end{aligned} \tag{3.11}$$

Next, we derive the recursive formula of g_k when $k > 2$. According to (3.4),

$$g_{n-m-1} = 2\sin(2m+3)\alpha \cdot B_{m+1}/B_{m+2}. \tag{3.12}$$

Let $k = n-(m+1)$, then $g_{n-m-1} = g_k$ and $g_{n-m+1} = g_{k-2}$. After the calculation (3.12) $\div$ (3.4), the recursive relation between g_k and g_{k-2} when $k > 2$ can be obtained:

$$\begin{aligned} g_k &= \lambda_k \cdot g_{k-2}, \\ \lambda_k &= \frac{\sin(2k-1)\alpha}{\sin(2k-5)\alpha} \cdot \frac{\delta^2 + 2\delta\cos 2(k-2)\alpha + 1}{\delta^2 + 2\delta\cos 2(k-1)\alpha + 1}. \end{aligned} \tag{3.13}$$

With the derivations of (3.9), (3.10), (3.11), and (3.13), we can obtain any g_k $(0 \le k \le n)$. The conclusions of Section II show that connections exist between g_k and the impedance of the corresponding components (L_k or C_k). In the following parts, we deduce passband parameters and all unknown component values of the matching network according to (3.9), (3.10), (3.11), (3.13), (2.14), and the known parameters of the given transducer.

Firstly, by substituting (3.9), (3.10), and (3.11) into (2.14), through elimination method, we can obtain the following equation regardless of the parity of n:

$$\delta^2 + 2\frac{1+(2-\sigma)\cos 2\alpha}{1-\sigma+2\cos 2\alpha} + 1 = 0, \tag{3.14}$$

where $\sigma = R_1^2 C_2/L_1$ is the electrical property constant of the given transducer. The expression $\delta = (1-K_n)^{1/2n}$ and the power output characteristics of Butterworth filter indicates that the maximum attainable gain constant $K_n = 1-\delta^{2n}$ and $0 < K_n \le 1$, then $|\delta| < 1$. Considering that, (3.14) has only one specific root:

$$\delta = \sqrt{\left[\frac{1+(2-\sigma)\cos 2\alpha}{1-\sigma+2\cos 2\alpha}\right]^2 - 1} - \frac{1+(2-\sigma)\cos 2\alpha}{1-\sigma+2\cos 2\alpha}. \tag{3.15}$$

To a specific transducer, R_1, L_1, C_1, C_2, α, and δ are determined constants in the case of certain matching network order n. All unknown component values and passband characteristics of the matching network can be figured out and expressed with these constants (see Table 1).

TABLE 1. Calculation formulas of the matching network parameters and electronic component values.

Symbol	Derivation basis	Calculation formula
K_n	$\delta = (1-K_n)^{1/2n}$	$1-\delta^{2n}$.
BW_n	(2.14), (3.9), $y = p/BW_n$	$2R_1 \sin\alpha/[L_1(1+\delta)]$.
R_S	(2.14), (3.10)	$\begin{cases} R_1\cdot(1-\delta^n)/(1+\delta^n), & n \text{ is odd} \\ R_1\cdot(1+\delta^n)/(1-\delta^n). & n \text{ is even} \end{cases}$
L_k	(2.14), (3.13), (2.3)	$\begin{cases} \lambda_k L_{k-2}, & k\geq 3,\ k \text{ is odd} \\ L_1C_1/C_k. & k\geq 2,\ k \text{ is even} \end{cases}$
C_k	(2.14), (3.13), (2.3)	$\begin{cases} L_1C_1/L_k, & k\geq 3,\ k \text{ is odd} \\ \lambda_k C_{k-2}. & k\geq 4,\ k \text{ is even} \end{cases}$

TABLE 2. Major performance indicators and equivalent electrical parameters of the given transducer.

f_s/kHz	Q_m	K_{eff}	R_1/Ω	L_1/mH	C_1/nF	C_2/nF
20.2	12.7	0.254	493	49.5	1.27	24.9

According to Table 1, $L_3, C_4, L_5, \ldots, C_{k-1}, L_k, C_{k+1}, \ldots$ of the low-pass prototype structure shown in Fig. 5 can be derived from (2.14) and (3.13). The component values represent the impedance of each circuit branch. In addition, it is necessary to use (2.3) to calculate the corresponding values of their conjugate components $C_3, L_4, C_5, \ldots, L_{k-1}, C_k, L_{k+1}, \ldots$ for extending the EIM method into the band-pass circuit shown in Fig. 4.

IV. SIMULATION AND EXPERIMENT

Based on the derivations in Section III, we can calculate an arbitrary order matching network that helps the power output characteristics of a given transducer meet Butterworth band-pass response. In this section, we perform the impedance matching for a given transducer according to (3.15) and Table 1. The matching effect is then analyzed through simulation and experiment.

A typical narrowband three laminated piezoelectric transducer for acoustic logging is selected for analysis, and its major performance indicators and equivalent electrical parameters (measured by HP 4294A) at room temperature (25 °C) are shown in Table 2. Where f_s is the series resonant frequency and $f_s = \omega_s/2\pi$, Q_m is the mechanical quality factor, and K_{eff} is the effective electro-mechanical coupling coefficient. Besides, R_1, L_1, C_1, and C_2 represent the equivalent electronic component values of the transducer BVD model.

By substituting the parameters in Table 2 into the calculation formulas in Table 1, we can obtain the -3-dB (half-power) bandwidth $bw_n = BW_n/2\pi$, the maximum attainable gain constant K_n, and the other unknown components in the matching network (see Table 3).

TABLE 3. Theoretical parameters and electronic component values of the EIM network.

n	K_n	bw_n/kHz	R_S/Ω	L_k/mH	C_k/nF
2	0.876	5.51	1029	$L_2 = 2.50$	
3	0.783	7.06	1354	$L_2 = 2.50$ $L_3 = 17.2$	$C_3 = 3.64$
4	0.756	7.50	1454	$L_2 = 2.50$ $L_3 = 36.3$ $L_4 = 10.3$	$C_3 = 1.73$ $C_4 = 6.07$
5	0.745	7.67	1499	$L_2 = 2.50$ $L_3 = 45.8$ $L_4 = 4.70$ $L_5 = 10.3$	$C_3 = 1.37$ $C_4 = 13.2$ $C_5 = 6.10$

Taking the center frequency $\omega_c = \omega_s$ and rewriting (2.1), we can express the TPG function as

$$G(f) = \frac{K_n}{1 + [(f_s/w_n)(f/f_s - f_s/f)]^{2n}}. \tag{4.1}$$

where f is excitation frequency. According to (4.1), a group of theoretical curves of $G(f)$ that vary with the matching order n are obtained, as shown in Fig. 7.

Fig. 7 shows that the TPG curves of the transducer are flat in the passband. The larger the matching order is, the better the flatness will be. In theory, the maximum TPG is obtained at the series resonant frequency of the transducer, and the maximum value equals to K_n at the corresponding matching order. Compared with the case without any matching circuit, bw_n is increased by 217%, 306%, 331%, and 341% when the matching order n varies, and K_n is increased by 167%, 139%, 130%, and 127%, respectively.

To verify the theoretical results, we performed software simulation and experiment. Firstly, according to the circuit structure in Fig. 4 and the calculated component values in Table 3, we use an EDA software (NI multisim 14.0) to construct the transducer matching circuits with different orders. Based on BVD model, the active power is only consumed by R_L (R_1), then

$$G(f) = P_L/P_A, \tag{4.2}$$

where P_A is the available power of the signal source, which is equal to half of the total power of the signal source according to maximum power transfer theorem, that is

$$P_A = (|E_S|/\sqrt{2})^2/4R_S = |E_S|^2/8R_S. \tag{4.3}$$

Let the peak–peak voltage on R_L be V_L, then

$$P_L = (|V_L|/\sqrt{2})^2/R_L = |V_L|^2/2R_L, \tag{4.4}$$

and (4.2) can be rewritten as

$$G(f) = 4(R_S/R_L)(V_L/E_S)^2. \tag{4.5}$$

In simulation,R_S, R_L, and E_S are all constants, and (4.5) indicates that the simulation results of TPG can be obtained

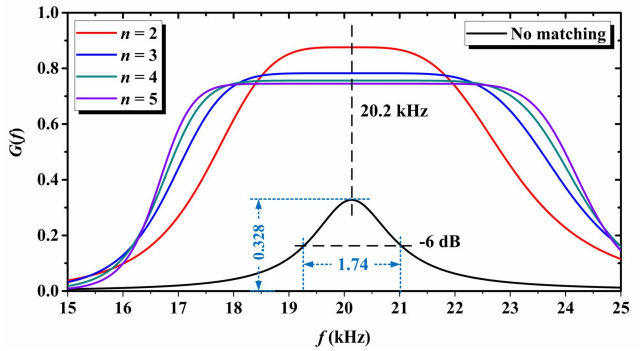

FIGURE 7. Theoretical TPG curves of the given transducer at different matching orders.

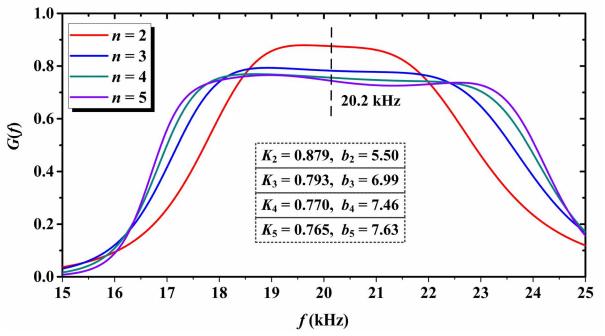

FIGURE 8. Simulated TPG curves of the given transducer at different matching orders.

by detecting V_L. Fig. 8 shows that the shapes of the simulation curves are similar to those of Fig. 7, and K_n and bw_n are close to the theoretical results in Table 3.

We then investigate the transmission characteristics of the matching network N. The circuit system in Fig. 5 is viewed as a combination of two terminals and a lossless two-port network. According to the theoretical component values in Table 3, we construct the testing circuits with an EDA software (ADS 2019) and obtain the simulated S-parameters of the matching network (see Fig. 9).

The theoretical calculations and simulation results (TPG curves and S-parameters) show that the bandwidth bw_n increases and the TPG curves become flat with the increase of matching order n. However, the maximum attainable gain constant K_n decreases. When $n > 3$, the changes in bw_n and K_n are no longer significant, and the complexity of the matching circuit increases. Considering the frequency drift of the given transducer is 2.8 kHz within the temperature range of 25–175°C, while the theoretical calculations and simulation results show that bw_n is larger than the drift value regardless of the matching order. Thus, the proposed matching network of arbitrary matching order can meet the broadband matching requirements of the given transducer. Here, we only perform the verification experiments on a third-order matching network.

As shown in Fig. 10 and Fig. 11, the experimental system mainly consists of a waveform generator (output impedance is 50 Ω), an oscilloscope, a piezoelectric transducer, and the

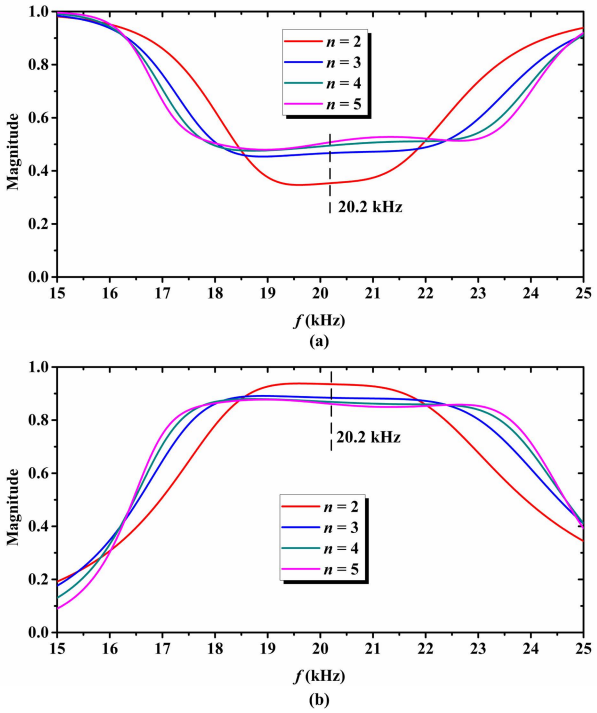

FIGURE 9. S-parameter simulation results of the lossless two-port matching network. (a) S11, (b) S21.

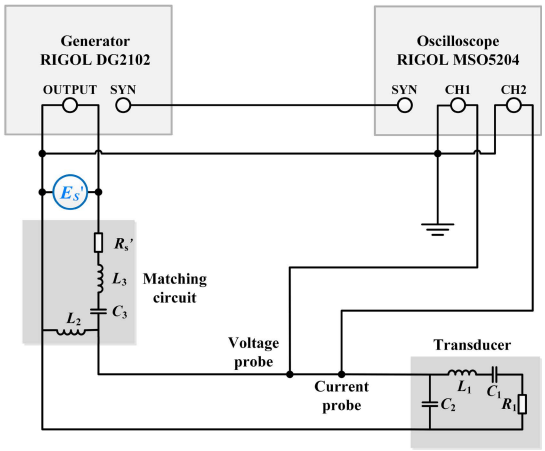

FIGURE 10. Structure of the TPG experimental system.

matching circuit. The transducer adopted in the experiment is the same as that used in the above simulation. Thus, the main performance indicators and impedance curve are also presented in Table 2 and Fig. 7, respectively.

The voltage and current probes measure the voltage V_T on the transducer and the current I_T flowing through the transducer, respectively. The oscilloscope records the real time output voltage E_S', values of V_T and I_T, and the phase angle φ between V_T and I_T. Then, the experimental results of TPG can be obtained with

$$G(f) = 4R_S V_T I_T \cos\varphi \Big/ (E_S')^2, \tag{4.6}$$

where f is evaluated at discrete points between 15 and 25 kHz, with 1 kHz step. The signal source is used to generate

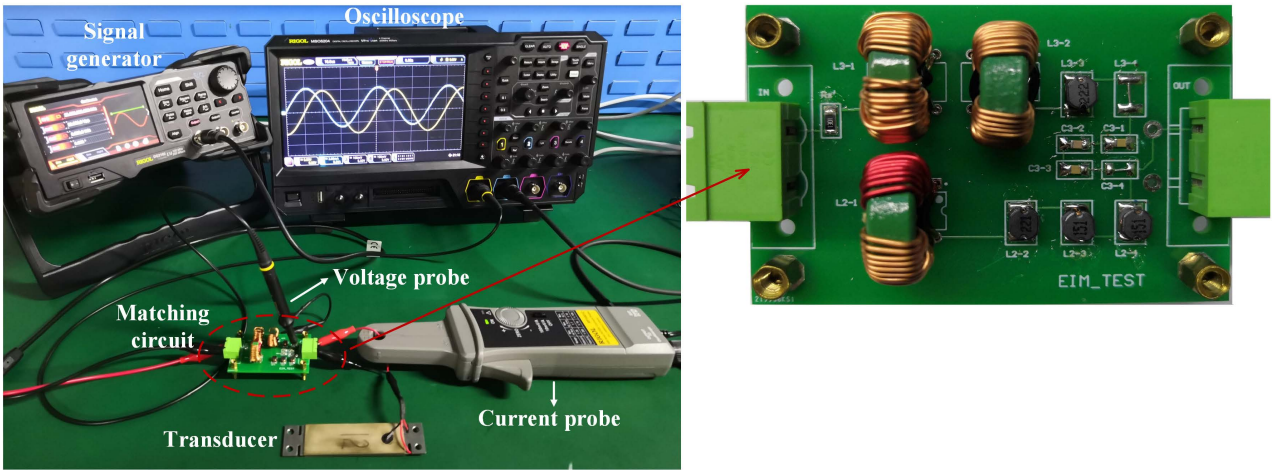

FIGURE 11. Picture of the experimental setup and the EIM circuit board.

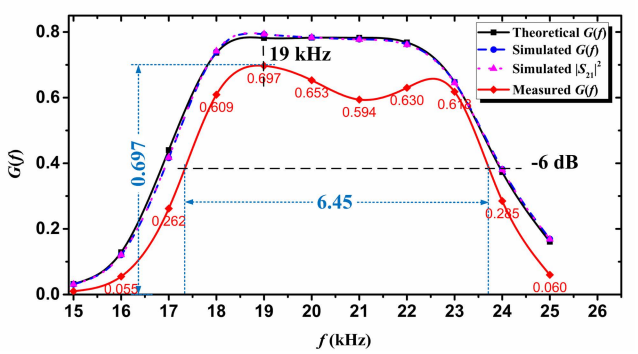

FIGURE 12. Comparison of theoretical calculation, simulation, and experimental results.

TABLE 4. Component Value error of the matching circuit.

	R_S/Ω	L_2/mH	L_3/mH	C_3/nF
Theoretical value	1352	2.50	17.2	3.64
Nominal value	1350	2.52	17.2	3.63
Measured value	1350	2.37	16.8	3.75
Error	0.1%	-5.2%	-2.3%	3.0%

continuous sinusoidal signals at various frequencies to excite the transducer. E_S', V_T, I_T, and φ are measured, and the TPG curves of the transducer are then obtained.

The comparison of theoretical calculation, simulation, and experimental results are shown in Fig. 12. It can be seen that both the simulation results of TPG and S-parameters are close to the theoretical calculations. The curves of $G(f)$ and $|S_{21}|^2$ are almost coincident, which conforms to the theoretical derivation of (2.6). Compared with theoretical calculations, the experimental errors of bw_n and K_n are –8.6% and –10.7%, respectively.

The measured $G(f)$ curve takes maximum at 19.0 kHz instead of the series resonant frequency (20.2 kHz) of the transducer. Besides, a significant fluctuation is observed in the passband.

The main reasons for deviation between the experimental and theoretical results are as follows: 1. The curves in Fig. 1 are measured with an impedance analyzer (Agilent 4294A), and based on that, the parameters of the given transducer in Table 2 are calculated with computing formulas. Therefore, errors are introduced in both processes of curve measurement and parameter calculation. 2. The actual signal generator is non-ideal, its internal resistance cannot be ignored, and the existence of internal resistance will affect the actual output voltage. 3. Since the value of electronic components used for EIM is not nominal, we need to combine the conventional components in series and/or parallel to produce the matching components that required for the experiment. Thus, there are errors between the combined components and the theoretical ones. Table 4 presents the error between the measured value and the theoretical value. 4. For the limitation of measuring accuracy, the measurement errors introduced by probes, especially the current probe, are inevitable. 5. The resistance and stray inductance on connection wires also affect the experimental results.

V. CONCLUSION

The dominant frequency drift of piezoelectric transducer is unfavorable to the excitation efficiency and the stability of AE system. This condition also limits the application of piezoelectric transducer in specific areas, such as acoustic well-logging, where the ambient temperature dramatically changes. To broaden the operating bandwidth of the narrowband transducers, we propose a broadband impedance matching method based on Butterworth filtering response. According to BVD model and measured impedance parameters, the transducer can be viewed as a simple RLC load, then the AE system becomes a circuit combination of two terminals and a lossless two-port network.

Under these conditions, reference [15] use a computerized Smith chart to establish the parameters of the EIM network, while references [16] and [18] use the analytical methods to calculate the value of electronic components and give a transducer EIM of third-order filter form.

Deferent from the above methods, we give an analytical method for EIM of arbitrary order n, instead of just getting a typical third-order matching network. In this way, the complex broadband matching becomes a relatively simple mathematical problem. Compared with the situation without impedance matching, this method can theoretically broaden the bandwidth of the given transducer by at least 217% and increase the maximum attainable gain by at most 167% (when $n = 2$). As a result, the broadened bandwidth can cover the frequency drift range of the given transducer. It should be noted that the complexity of the matching circuit increases, but the changes in EIM performance are no longer significant when $n > 3$.

To verify the method, we adopt different EDA methods to simulate the TPG characteristics of the matched transducer and the S-parameters of the matching network. The simulation results show that the curves of $G(f)$ and $|S_{21}|^2$ obtained by the two different simulation methods are almost coincident, and both of them are close to the theoretical results. An experimental system is then established to measure the performance of TPG. The results show that the bandwidth and the maximum attainable gain are improved by 271% and 112%, respectively, owing to this third-order matching circuit. Although errors between experimental results and theoretical calculations are detected, the measured TPG curve is similar to the theoretical one and keeps a good flatness in the passband.

APPENDIX I

The proving process of (3.3) to (3.8) is divided into three stages: I. Decomposing the expressions of A_0 and A_1, using Euclidean algorithm to obtain A_2, A_3, andA_4, then verifying (3.3) to (3.7) when $m = 1, 2,$ 3.II. Using the mathematical induction to verify that for any $m(m > 3)$, (3.3) to (3.7) are still valid. III. Using the proven conclusions of (3.7) and root-finding algorithm to obtain the expressions of B_n and B_{n-1}, for verifying (3.8).

A. STAGE I

Step 1. According to the format of (3.3) and the geometric progression summation equation

$$1 - \delta^k = (1 - \delta) \sum_{p=0}^{k-1} \delta^p,$$

A_1can be expressed as

$$A_1 = B_1 \sum_{k=1}^{n} a_k C_{1,k} D_{1,k} y^{n-k}, \tag{APX.1}$$

where

$$B_1 = 1 - \delta, C_{1,k} = 1, D_{1,k} = \sum_{p=0}^{k-1} \delta^p. \tag{APX.2}$$

By extracting the first two terms of A_0 and A_1, (3.2) can be rewritten as the following forms:

$$A_0 = S_0 + \sum_{k=2}^{n} a_k (1 + \delta^k) y^{n-k}, \tag{APX.3}$$

$$A_1 = S_1 + \sum_{k=3}^{n} a_k (1 - \delta^k) y^{n-k}, \tag{APX.4}$$

where

$$S_0 = 2 \left(y + \frac{1 + \delta}{2 \sin \alpha} \right) y^{n-1}, \tag{APX.5}$$

$$\begin{aligned} S_1 &= \frac{B_1}{\sin \alpha} \left(y + \frac{1 + \delta}{2 \sin \alpha} \right) y^{n-2} \\ &= a_1 B_1 C_{1,1} \left(y + \frac{1 + \delta}{2 \sin \alpha} \right) y^{n-2}. \end{aligned} \tag{APX.6}$$

(APX.5) and (APX.6) show the existence of a common factor $y + (1 + \delta)/2 \sin \alpha$ in S_0 and S_1. Thus, the equation $A_0/A_1 - A_2/A_1 = g_n y$ exhibits that the order of A_2 is one lower than that of A_1, and

$$g_n = 2 \sin \alpha \cdot \frac{1}{B_1}, \tag{APX.7}$$

$$\begin{aligned} A_2 &= A_0 - g_n A_1 y \\ &= \sum_{k=2}^{n} a_k (1 + \delta^k) y^{n-k} - g_n \sum_{k=3}^{n} a_k (1 - \delta^k) y^{n-k+1}. \end{aligned} \tag{APX.8}$$

Step 2. According to (APX.7), polynomial coefficients features in (2.9), transformation $k = k' + 1$, and equation

$$1 - \delta^{k+1} = (1 - \delta) \sum_{p=0}^{k} \delta^p,$$

(APX.8) can be rewritten as

$$A_2 = B_2 \sum_{k=2}^{n} a_k C_{2,k} D_{2,k} y^{n-k}, \tag{APX.9}$$

where

$$\begin{aligned} B_2 &= \delta^2 - 2\delta \cos 2\alpha + 1, \\ C_{2,k} &= \frac{\sin(k-1)\alpha}{\sin(k+1)\alpha}, \\ D_{2,k} &= \sum_{p=0}^{k-2} \frac{\sin(p+1)\alpha}{\sin \alpha} \cdot \frac{\sin(k-p-1)\alpha}{\sin(k-1)\alpha} \cdot \delta^p. \end{aligned} \tag{APX.10}$$

The sum of the first two terms of A_2 is

$$\begin{aligned} S_2 &= a_2 B_2 \frac{\sin \alpha}{\sin 3\alpha} \left(y + \frac{1 + \delta}{2 \sin \alpha} \right) y^{n-3} \\ &= a_2 B_2 C_{2,2} \left(y + \frac{1 + \delta}{2 \sin \alpha} \right) y^{n-3}. \end{aligned} \tag{APX.11}$$

(APX.6) and (APX.11) show the existence of a common factor $y + (1+\delta)/2\sin\alpha$ in S_1 and S_2. Thus, the equation $A_1/A_2 - A_3/A_2 = g_{n-1}y$ exhibits that the order of A_3 is one lower than that of A_2, and

$$g_{n-1} = \frac{a_1}{a_2}\cdot\frac{C_{1,1}}{C_{2,2}}\cdot\frac{B_1}{B_2} = 2\sin 3\alpha\cdot\frac{B_1}{B_2}, \quad \text{(APX.12)}$$

$$\begin{aligned} A_3 &= A_1 - g_{n-1}A_2 y \\ &= B_1\sum_{k=3}^{n} a_k C_{1,k} D_{1,k} y^{n-k} \\ &\quad - g_{n-1}B_2\sum_{k=4}^{n} a_k C_{2,k} D_{2,k} y^{n-k+1}. \end{aligned} \quad \text{(APX.13)}$$

Step 3. In the same way as step 2, (APX.13) is rewritten as

$$A_3 = B_3\sum_{k=3}^{n} a_k C_{3,k} D_{3,k} y^{n-k}. \quad \text{(APX.14)}$$

where

$$\begin{aligned} B_3 &= (\delta^2 - 2\delta\cos 4\alpha + 1)\cdot B_1, \\ C_{3,k} &= \frac{\sin(k-1)\alpha}{\sin(k+1)\alpha}\cdot\frac{\sin(k-2)\alpha}{\sin(k+2)\alpha}, \\ D_{3,k} &= \sum_{p=0}^{k-3}\prod_{q=1}^{2}\frac{\sin(p+q)\alpha}{\sin q\alpha}\cdot\frac{\sin(k-p-q)\alpha}{\sin(k-q)\alpha}\cdot\delta^p. \end{aligned} \quad \text{(APX.15)}$$

The sum of the first two terms of A_3 is

$$\begin{aligned} S_3 &= a_3 B_3\frac{\sin 2\alpha}{\sin 4\alpha}\cdot\frac{\sin\alpha}{\sin 5\alpha}\left(y + \frac{1+\delta}{2\sin\alpha}\right) y^{n-4} \\ &= a_3 B_3 C_{3,3}\left(y + \frac{1+\delta}{2\sin\alpha}\right) y^{n-4}. \end{aligned} \quad \text{(APX.16)}$$

(APX.11) and (APX.16) show the existence of a common factor $y + (1+\delta)/2\sin\alpha$ in S_2 and S_3. Thus, the equation $A_2/A_3 - A_4/A_3 = g_{n-2}y$ exhibits that the order of A_4 is one lower than that of A_3, and

$$g_{n-2} = \frac{a_2}{a_3}\cdot\frac{C_{2,2}}{C_{3,3}}\cdot\frac{B_2}{B_3} = 2\sin 5\alpha\cdot\frac{B_2}{B_3}, \quad \text{(APX.17)}$$

$$\begin{aligned} A_4 &= A_2 - g_{n-2}A_3 y \\ &= B_2\sum_{k=3}^{n} a_k C_{2,k} D_{2,k} y^{n-k} \\ &\quad - g_{n-2}B_3\sum_{k=5}^{n} a_k C_{3,k} D_{3,k} y^{n-k+1}. \end{aligned} \quad \text{(APX.18)}$$

According to the above derivations and conclusions, A_m and $g_{n-m+1}(m = 1, 2, 3)$ can be obtained, (3.3) to (3.7) are then verified in the case of $m = 1, 2, 3$.

B. STAGE II

By mathematical induction, assuming that (3.3) to (3.7) are tenable for any m $(m > 3)$, then the equations are valid if we verify that they are still tenable for $m+1$. Hence, first we need to obtain the expression of A_{m+1}.

In the same way as Stage I, by extracting the first two terms of A_{m-1} and A_m, the polynomials can be rewritten as

$$\begin{aligned} A_{m-1} &= S_{m-1} + B_{m-1}\sum_{k=m-1+2}^{n} a_k C_{m-1,k} D_{m-1,k} y^{n-k}, \\ A_m &= S_m + B_m\sum_{k=m+2}^{n} a_k C_{m,k} D_{m,k} y^{n-k}, \end{aligned} \quad \text{(APX.19)}$$

where

$$\begin{aligned} S_{m-1} &= a_{m-1}B_{m-1}C_{m-1,m-1}\left(y + \frac{1+\delta}{2\sin\alpha}\right) y^{n-(m-1)-1}, \\ S_m &= a_m B_m C_{m,m}\left(y + \frac{1+\delta}{2\sin\alpha}\right) y^{n-m-1}. \end{aligned} \quad \text{(APX.20)}$$

(APX.20) shows that the factor $y + (1+\delta)/2\sin\alpha$ also exists in expressions ofS_{m-1} and S_m. Thus, the equation $A_{m-1}/A_m - A_{m+1}/A_m = g_{n-m+1}y$ exhibits that the order of A_{m+1} is one lower than that of A_m, and

$$\begin{aligned} g_{n-m+1} &= \frac{a_{m-1}}{a_m}\cdot\frac{C_{m-1,m-1}}{C_{m,m}}\cdot\frac{B_{m-1}}{B_m} \\ &= 2\sin(2m-1)\alpha\cdot\frac{B_{m-1}}{B_m}, \end{aligned} \quad \text{(APX.21)}$$

$$\begin{aligned} A_{m+1} &= A_{m-1} - g_{n-m+1}A_m y \\ &= B_{m-1}\sum_{k=m+1}^{n} a_k C_{m-1,k} D_{m-1,k} y^{n-k} \\ &\quad - g_{n-m+1}B_m\sum_{k=m+2}^{n} a_k C_{m,k} D_{m,k} y^{n-k+1}. \end{aligned} \quad \text{(APX.22)}$$

According to (APX.21), polynomial coefficients feature in (2.9), and transformation $k = k' + 1$,(APX.22) is rewritten as:

$$A_{m+1} = B_{m-1}\sum_{k=m+1}^{n} a_k E_{m+1,k} y^{n-k}, \quad \text{(APX.23)}$$

where

$$\begin{aligned} E_{m+1,k} &= C_{m-1,k}D_{m-1,k} \\ &\quad -2\sin(2m-1)\alpha\cdot\frac{\cos k\alpha}{\sin(k+1)\alpha}\cdot C_{m,k+1}D_{m,k+1}. \end{aligned} \quad \text{(APX.24)}$$

$C_{m-1,k}$, $D_{m-1,k}$, $C_{m,k+1}$, and $D_{m,k+1}$ are obtained on the basis of (3.5), (3.6), and (3.7). By substituting these equations into (APX.23) and (APX.24), then simplifying the equations with trigonometric functions, the expression of A_{m+1} is then obtained:

$$A_{m+1} = B_{m+1}\sum_{k=m+1}^{n} a_k C_{m+1,k} D_{m+1,k} y^{n-k}, \quad \text{(APX.25)}$$

where

$$B_{m+1} = (\delta^2 - 2\delta\cos 2m\alpha + 1)B_{m-1},$$

$$C_{m+1,k} = \prod_{p=1}^{(m-1)+1} \frac{\sin(k-p)\alpha}{\sin(k+p)\alpha},$$

$$D_{m+1,k} = \sum_{p=0}^{k-(m+1)} \prod_{q=1}^{(m-1)+1} \frac{\sin(p+q)\alpha}{\sin q\alpha} \cdot \frac{\sin(k-p-q)\alpha}{\sin(k-q)\alpha} \cdot \delta^p. \quad \text{(APX.26)}$$

(APX.21), (APX.25), and (APX.26) show that (3.3) to (3.7) are still tenable for $m+1$, indicating that these equations are valid for any m ($m > 3$).

C. STAGE III

(3.8) is a special case of (3.7) when $m = n$, and the values of B_n and B_{n-1} depend on the parity of matching order n. When n is even, let $n = 2m$ and $\alpha = \pi/4m$. Then, (3.7) can be rewritten as:

$$\begin{aligned} B_n = B_{2m} &= \prod_{k=1}^{m} \left\{\delta^2 - 2\delta\cos[(2k-1)\pi/2m] + 1\right\} \\ &= \prod_{k=0}^{m-1} \left\{\delta^2 - 2\delta\cos[(2k-1)\pi/2m] + 1\right\}. \end{aligned} \quad \text{(APX.27)}$$

Let $\beta = \exp(j\pi/2m)$, $X_k = \delta^2 - 2\delta\cos[(2k+1)\pi/2m] + 1$, and $Y_k = \delta - \beta^{2k+1}$. Then for any k ($k < m$), the equation as follows is obtained:

$$\begin{aligned} X_k &= (\delta - \beta^{2k+1}) \cdot [\delta - \beta^{2(2m-1-k)+1}] \\ &= Y_k \cdot Y_{2m-1-k}. \end{aligned} \quad \text{(APX.28)}$$

Substituting (APX.28) into (APX.27), then (APX.27) can be rewritten as

$$\begin{aligned} B_n &= \prod_{k=0}^{m-1} X_k = \prod_{k=0}^{m-1} Y_k \cdot Y_{2m-1-k} = \prod_{k=0}^{2m-1} Y_k \\ &= \prod_{k=0}^{2m-1} \left\{\delta - \exp[j(2k+1)\pi/2m]\right\}. \end{aligned} \quad \text{(APX.29)}$$

According to root-finding algorithm, Y_k is a characteristic root of equation $f(\delta) = \delta^{2m} + 1$, that is

$$\delta^{2m} + 1 = \prod_{k=0}^{2m-1} \left\{\delta - \exp[j(2k+1)\pi/2m]\right\}. \quad \text{(APX.30)}$$

$$B_n = \delta^{2m} + 1 = \delta^n + 1. \quad \text{(APX.31)}$$

Then, according to (3.7),

$$B_{n-1} = B_{2m-1} = (1-\delta) \prod_{k=1}^{m-1} [\delta^2 - 2\delta\cos(k\pi/m) + 1]. \quad \text{(APX.32)}$$

Multiply both sides of the equal sign of (APX.32) by a constant $-(\delta+1)$, then

$$-(\delta+1) B_{n-1} = (\delta-1)(\delta+1) \prod_{k=1}^{m-1} [\delta^2 - 2\delta\cos(k\pi/m) + 1]. \quad \text{(APX.33)}$$

Let $X_k = \delta^2 - 2\delta\cos(k\pi/m) + 1$ and $Y_k = \delta - \beta^{2k}$. Then for any k ($k \le m$), the equation as follows is obtained:

$$X_k = (\delta - \beta^{2k}) \cdot [\delta - \beta^{2(2m-k)}] = Y_k \cdot Y_{2m-k}, \quad \text{(APX.34)}$$

Substituting (APX.34) into (APX.33), then (APX.33) can be rewritten as

$$\begin{aligned} -(\delta+1) B_{n-1} &= (\delta^2 - 1) \prod_{k=1}^{m-1} X_k \\ &= Y_0 Y_m \cdot Y_1 Y_{2m-1} \cdot \ldots \cdot Y_k Y_{2m-k} \ldots \\ &= \prod_{k=0}^{2m-1} Y_k = \prod_{k=0}^{2m-1} [\delta - \exp(jk\pi/m)]. \end{aligned} \quad \text{(APX.35)}$$

Root-finding algorithm indicates that Y_k is a characteristic root of equation $f(\delta) = \delta^{2m} - 1$, that is

$$\delta^{2m} - 1 = \prod_{k=0}^{2m-1} [\delta - \exp(j2k\pi/2m)] \quad \text{(APX.36)}$$

$$B_{n-1} = (1-\delta^n)/(1+\delta). \quad \text{(APX.37)}$$

In conclusion, (3.8) is valid when n is even. When n is an odd number, the proof is similar to the above process and no elaboration will be provided here.

REFERENCES

[1] R. Khazaka, L. Mendizabal, D. Henry, and R. Hanna, "Survey of high-temperature reliability of power electronics packaging components," *IEEE Trans. Power Electron.*, vol. 30, no. 5, pp. 2456–2464, May 2015.

[2] M. A. Huque, S. K. Islam, L. M. Tolbert, and B. J. Blalock, "A 200 °C universal gate driver integrated circuit for extreme environment applications," *IEEE Trans. Power Electron.*, vol. 27, no. 9, pp. 4153–4162, Sep. 2012.

[3] R. K. Traeger and P. C. Lysne, "High temperature electronics application in well logging," *IEEE Trans. Nucl. Sci.*, vol. NS-35, no. 1, pp. 852–854, Feb. 1988.

[4] Z. Jin, L. Huo, T. Long, X. Guo, J. Tu, and D. Zhang, "An online impedance analysis and matching system for ultrasonic transducers," *IEEE Trans. Ultrason., Ferroelectr., Freq. Control*, vol. 66, no. 3, pp. 591–599, Mar. 2019.

[5] C. Song, Y. Huang, J. Zhou, P. Carter, S. Yuan, Q. Xu, and Z. Fei, "Matching network elimination in broadband rectennas for high-efficiency wireless power transfer and energy harvesting," *IEEE Trans. Ind. Electron.*, vol. 64, no. 5, pp. 3950–3961, May 2017.

[6] M. Fernandez, S. V. Hoeye, C. Vazquez, L. A. Gonzalez, and F. Las-Heras, "On the design of broadband hybrid amplifiers using non-uniform transmission lines as impedance matching networks," *IEEE Access*, vol. 7, pp. 19670–19677, 2019.

[7] J. An, K. Song, S. Zhang, J. Yang, and P. Cao, "Design of a broadband electrical impedance matching network for piezoelectric ultrasound transducers based on a genetic algorithm," *Sensors*, vol. 14, no. 4, pp. 6828–6843, Apr. 2014.

[8] X. Hu, X. Meng, C. Yu, and Y. Liu, "Design of highly efficient broadband harmonic-optimised GaN power amplifier via modified simplified real frequency technique," *Electron. Lett.*, vol. 53, no. 21, pp. 1414–1416, Oct. 2017.

[9] Z. Dai, S. He, J. Pang, J. Peng, C. Huang, and F. You, "Sub-optimal matching method for dual-band class-J power amplifier using real frequency technique," *IET Microw., Antennas Propag.*, vol. 11, no. 9, pp. 1218–1226, 2017.

[10] M. G. Kim, S. Yoon, H. H. Kim, and K. K. Shung, "Impedance matching network for high frequency ultrasonic transducer for cellular applications," *Ultrasonics*, vol. 65, pp. 258–267, Feb. 2016.
[11] X. Meng, C. Yu, Y. Liu, Y. Wu, X. Wang, and J. Wang, "Implementation of flat gain broadband power amplifier with impedance rotation compensation," *IEEE Access*, vol. 7, pp. 13304–13316, 2019.
[12] R. M. Fano, "Theoretical limitations on the broadband matching of arbitrary impedances," *J. Franklin Inst.*, vol. 249, no. 2, pp. 139–154, Feb. 1950.
[13] W.-K. Chen, "Explicit formulas for the synthesis of optimum broad-band impedance-matching networks," *IEEE Trans. Circuits Syst.*, vol. CAS-24, no. 4, pp. 157–169, Apr. 1977.
[14] H. Dedieu, C. Dehollaini, J. Neirynck, and G. Rhodes, "A new method for solving broadband matching problems," *IEEE Trans. Circuits Syst. I, Fundam. Theory Appl.*, vol. 41, no. 9, pp. 561–571, Sep. 1994.
[15] H. Y. Huang and D. Paramo, "Broadband electrical impedance matching for piezoelectric ultrasound transducers," *IEEE Trans. Ultrason., Ferroelectr., Freq. Control*, vol. 58, no. 12, pp. 2699–2707, Dec. 2011.
[16] H. Zhang, F. Wang, Y. Tian, X. Zhao, D. Zhang, and L. Han, "Electrical matching of low power piezoelectric ultrasonic transducers for microelectronic bonding," *Sens. Actuators A, Phys.*, vol. 199, pp. 241–249, Sep. 2013.
[17] Y. Yao, X. Ju, J. Lu, and B. Men, "Acoustic emission and echo signal compensation techniques applied to an ultrasonic logging-while-drilling caliper," *Sensors*, vol. 17, no. 6, p. 1351, 2017.
[18] J.-Y. Moon, J. Lee, and J. H. Chang, "Electrical impedance matching networks based on filter structures for high frequency ultrasound transducers," *Sens. Actuators A, Phys.*, vol. 251, pp. 225–233, Nov. 2016.
[19] D. Youla, "A new theory of broad-band matching," *IEEE Trans. Circuit Theory*, vol. CT-11, no. 1, pp. 30–50, Mar. 1964.
[20] W.-K. Chen and T. Chaisrakeo, "Explicit formulas for the synthesis of optimum bandpass Butterworth and Chebyshev impedance-matching networks," *IEEE Trans. Circuits Syst.*, vol. CAS-27, no. 10, pp. 928–942, Oct. 1980.

YONGCHAO YAO (Member, IEEE) received the B.S. degree in exploration technology and engineering from the China University of Petroleum (East China), Qingdao, China, in 2010, and the M.S. and Ph.D. degrees in geological resources and geological engineering from the China University of Petroleum (Beijing), Beijing, China, in 2013 and 2017, respectively.

He is currently a Postdoctoral Researcher with the Department of Earth and Space Sciences, Southern University of Science and Technology. His research interests include measurement and control technology, marine geophysics, industrial instrumentation, and acoustic well-logging.

BAOHAI TAN was born in Liaoning, China, in 1978. He received the B.S. degree in applied geophysics and the M.S. degree in geological resources and geological engineering from the China University of Petroleum (East China), Dongying, China, in 2001 and 2004, respectively.

He is currently an Associate Professor with the School of Geosciences, China University of Petroleum (East China). His research interests include acoustic logging instrument design, measurement, and control technology.

ZHANXIANG HE was born in Pingjiang County, Hunan, China, in 1962. He received the M.S. degree in applied geophysics from the China University of Geosciences, in 1989, and the Ph.D. degree in petroleum geophysical exploration from the Chengdu University of Technology, in 2006.

He was a Visiting Scholar with the University of Houston, from 2005 to 2006. From 1989 to 2018, he was an Engineer, a Senior Engineer, a Professor Level Senior Engineer, the Chief Engineer, and a Senior Technical Expert at Bureau of Geophysical Prospecting Inc., China National Petroleum Corporation. In 2018, he joined the Southern University of Science and Technology as a Research Professor. His research interests include geo-electromagnetics and integrated geophysics, deep underground structure research, and the exploration of geothermal, oil, gas, and mineral resources.

XIANPING LIU received the B.S. degree in exploration technology and engineering and the Ph.D. degree in geological resources and geological engineering from the China University of Petroleum (Beijing), Beijing, China, in 2009 and 2016, respectively.

He is currently a Senior Engineer at CNPC Logging Company Ltd., Tianjin Branch. His research interests include acoustic logging instrument design, measurement, and control technology.